

UC Berkeley

UC Berkeley Previously Published Works

Title

On multi-point gas injection to form an air layer for frictional drag reduction

Permalink

<https://escholarship.org/uc/item/886811vb>

Authors

Mäkiharju, Simo A
Ceccio, Steven L

Publication Date

2018

DOI

10.1016/j.oceaneng.2017.10.041

Peer reviewed



On multi-point gas injection to form an air layer for frictional drag reduction



Simo A. Mäkiharju^{a,*}, Steven L. Ceccio^b

^a University of California, Berkeley, CA 94720, USA

^b University of Michigan, Ann Arbor, MI 48109, USA

ARTICLE INFO

Keywords:

Gas injection
Multiphase
Frictional drag reduction
Air layer
Jet

ABSTRACT

Air layer drag reduction has been shown to be a feasible drag reducing technique at the laboratory and at full ship scales. In most studies, the air layers have been generated *via* gas injection from two-dimensional spanwise slots. However, given ship's structural considerations, it would be preferable to use discrete holes. The present study expands on the work on single orifice gas injection to multi-hole injection. When compared with slot injection, multi-point injection lead to a reduced range of gas fluxes that formed an air layer. Gas injected from a series of discrete holes can exhibit complex flow patterns, including roll-up into the core of liquid vortices that form as part of the process of injecting gas into the liquid boundary layer. The finite span and length of the model utilized for the present experiments was modest. It remains to be shown if a larger model with similar scaled up geometry (and with more beanwise holes) would enable the formation of a stable air layer with a gas flux per unit span that is similar to that required for slot injection. Nevertheless, the results presented here illustrate the complexity associated with gas injection through multiple perforations in a hull.

1. Introduction

Air Layer Drag Reduction (ALDR) has been shown to reduce the frictional drag by over 80% on the surface covered (Ceccio, 2010; Elbing et al., 2013; Mäkiharju et al., 2012). Similar results have been achieved also by Partial Cavity Drag Reduction (PCDR), which is a related technique with the rough distinction being that the “layer” (better described as a cavity) of gas is much thicker than the boundary layer. PCDR was investigated by Gokcay et al. (2004), Matveev (2007), Lay et al. (2010), Mäkiharju et al. (2013) and others. Distinctions between discrete bubble drag reduction, ALDR and PCDR techniques were more thoroughly described in Mäkiharju et al. (2012), and more recently a survey of some of the different frictional drag reduction techniques utilizing gas injection was also provided by Murai (2014). Also, Perlin and Ceccio (2014) reviews a wide variety of frictional drag reduction techniques, ranging from passive to active methods. However, in the present work we will focus solely on practical issues one may encounter when trying to practically implement ALDR.

In most ALDR experiments gas has been introduced *via* continuous spanwise slots that are either open or filled with porous material to ensure the creation of a nominally spanwise uniform gas layer. And, while an air layer may be generated utilizing such a slot with air forced solely by a compressor (e.g. Elbing et al., 2013), some authors have also

suggested use of hydrofoils below the slot to reduce the require air pumping power (e.g. Kumagai et al., 2015). Also, recent paper by Park et al. (2016) discusses nominally spanwise uniform gas injection to boundary layers. However, for practical application of ALDR it is desirable to implement the least complex arrangement for the introduction of the gas while maximizing the hull's structural integrity. Indeed, the simplest method (and one that may prove to be easiest to implement particularly if retrofitting an old hull) is to introduce the gas *via* a series of plain round orifices penetrating the hull. Such an injection configuration would produce a gas jet in liquid cross-flow. Despite its geometric simplicity, such an injection configuration can yield a quite complex multiphase flow.

Jets in cross-flows of similar fluids have been studied extensively, and a recent review was provided by Mahesh (2013). However, not much data is available on the complex flow resulting from the normal injection of a gas jet into a liquid cross-flow over the range of Reynolds and Froude numbers of interest. In particular, the Froude numbers for practical applications are such that the influence of buoyancy is significant, *i.e.* whereby the gas jet injected beneath a surface rises. The injection of gas from a single hole with gravity oriented streamwise was studied by Vigneau et al. (2001a, 2001b), and with gravity oriented normal to the surface (*i.e.* relevant for ALDR) by Lee (2015) and Mäkiharju et al. (2017). Lee (2015) and Mäkiharju et al. (2017) conducted studies to

* Corresponding author.

E-mail address: makiharju@berkeley.edu (S.A. Mäkiharju).

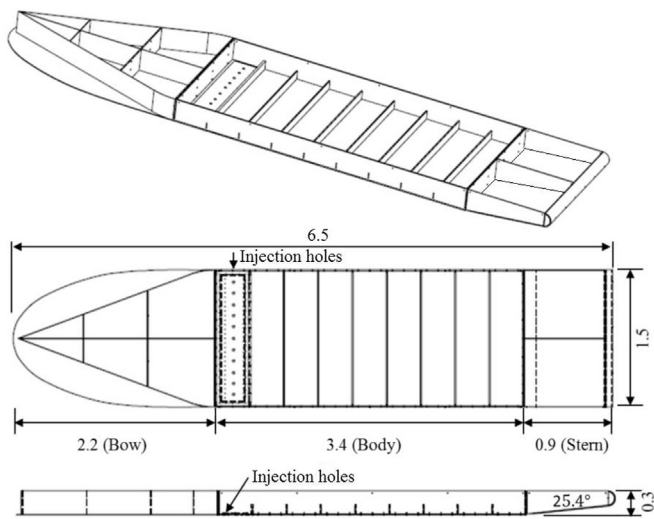


Fig. 1. A schematic diagram of the model used in the experiments (same as utilized by Lee, 2015; Mäkiharju et al., 2017). To reduce air leakage from the sides due to finite span of the model, adjustable strakes (set to be 7.5 cm tall) were installed on both sides of the model and extended from bow to stern (i.e. as measured from the bow: 2.2–5.4 m in streamwise direction). All dimensions listed in the figure are in meters, except where degrees are explicitly identified for the transom's rise angle.

examine gas injected into a cross flow from an orifice placed beneath a hull. For flows of moderate Froude number, buoyancy drives the ejected gas plume toward the hull surface downstream of the injection location, often creating a “V” shaped cavity. Under some conditions, the cavity forms two gas branches that are separated by a mainly liquid flow, or the region between the two legs may be filled with a thin layer of gas. The topology of the cavity is dependent on a variety of parameters, including the Froude, Reynolds, and Weber Number of the flow and the volume flow, mean velocity, and angle of the injected gas, the incoming boundary layer thickness, and the orifice diameter.

While injection from multiple holes for drag reduction was tested by Insel et al. (2010) on a towed ship model, the data presented did not yield generalizable answers nor were the gas fluxes likely sufficient to form an air layer, although the general features of the flows they report are similar to those observed in the present study.

In the present work, the ability to form an air layer using discrete multi-hole gas injection is investigated experimentally in a tow tank at Reynolds numbers $O(10^6)$, where Reynolds number is defined based on distance from the leading edge to gas injection location. This work expands on that reported by Lee (2015) and Mäkiharju et al. (2017) for gas injected from a single orifice by extending the study to include the interaction of multiple gas pockets formed by nominally uniform gas

injection. In Section 2 we will discuss the experimental setup. In Section 3 we briefly summarize single hole gas injection results from previous work by Mäkiharju et al. (2017), followed by Section 4 that present the multi hole gas injection data. We conclude in Section 5 with a brief summary discussion of the results and proposed future work.

2. Experimental setup

A 6.5 m long and 1.5 m wide barge with a flat bottom was utilized in the University of Michigan's Marine Hydrodynamics Laboratory physical modelling basin that is 109.7 m long, 6.7 m wide and 3.2 m deep. The model was designed to produce a near zero pressure gradient streamwise and nominally span-wise uniform turbulent boundary layer at the location of gas injection, which was found to be 54 ± 3 mm thick. To have a nominally two-dimensional inflow that is free of significant corner vortices, an elliptic leading edge shape was used on the flat plate that formed the bow. The draft of the model was such that the flat plate at the bow was always immersed below the surface, and a V-shape superstructure above this flat plate was used to deflect the liquid flow of the free surface away from the model that is shown in Fig. 1. The bow was followed by a 3.4 m long body that had a stiff aluminum structure and a flat bottom made of single seamless clear acrylic plastic to enable visualization through the bottom. The stern was a simple two-dimensional shape rising at an angle of 25.4° . The barge was mounted such that the flat bottom was nominally normal to gravity, and bottom angle was checked to be nominally zero with AccuRemote digital protractor with manufacturer specified accuracy of $\pm 0.2^\circ$. The surface roughness of the bottom of the bow and the acrylic plate of the body was measured using a Mitutoyo SJ-210 roughness meter. For the bow and acrylic plate we found surface roughness $[Ra, Rq]$ to be $[2.41, 3.92] \mu\text{m}$ and $[0.18, 0.33] \mu\text{m}$, respectively. Particles with $150 \mu\text{m}$ mean diameter were randomly scattered and affixed across the span of the model 1.7 m from the leading edge of the model on a 0.2 m wide strip to induce turbulent boundary layer transition upstream of the gas injection location.

As the focus of this study was on the effect of gas injection method on formation of an air layer, the barge was rigidly fixed to the carriage, and the draft of the model was held constant at 12 cm. For air layer drag reduction on a real ship, the situation would be further complicated by vessel motions and external flow which may have large perturbations, and these factors need to be further examined. During the measurement campaign, the model basin water temperature was nominally constant at 18°C . Between experiments, up to a 30 min pause was taken between runs to achieve nominally calm water condition. Compressed air was injected out of 1–6 pipes that had inside diameter, D_i , of 23.8 mm and a straight pipe section that was $38D_i$ long to achieve nominally fully developed turbulent pipe flow profile at the orifice exit. The pipes went through compression fittings and the injection plate, and terminated flush on the bottom surface of the gas injection plate. The pipe exits had

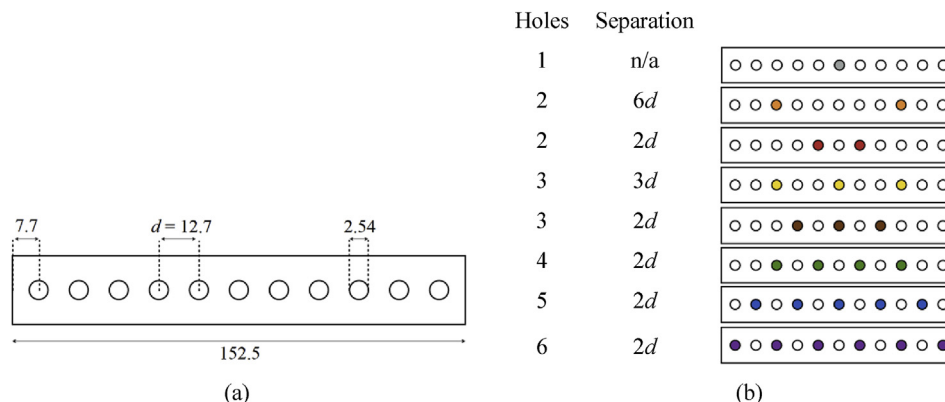


Fig. 2. Schematic diagrams of (a) the injection plate with dimensions in centimeters, and (b) the combinations of gas injection holes used.

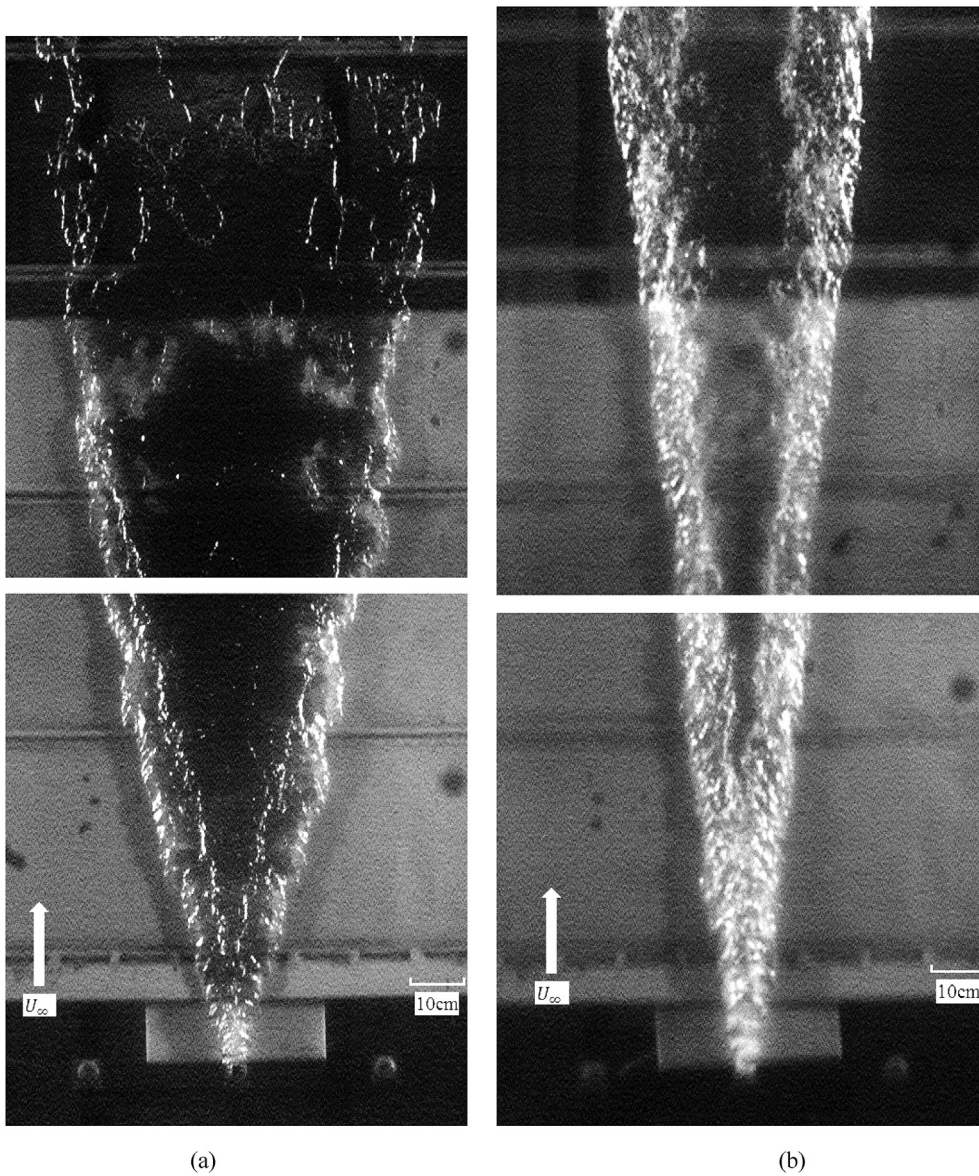


Fig. 3. A stitched image of (a) a Delta type gas pocket ($D_i \sim 20$ mm, $U_\infty = 2.0$ ms⁻¹, $Q_i = 4.3 \times 10^{-3}$ m³s⁻¹, $\delta = 53$ mm) and of (b) a Lambda type gas pocket ($D_i \cong 10$ mm, $U_\infty = 4.0$ ms⁻¹, $Q_i = 6.7 \times 10^{-3}$ m³s⁻¹, $\delta = 53$ mm). Figures adapted from Mäkiharju et al. (2017).

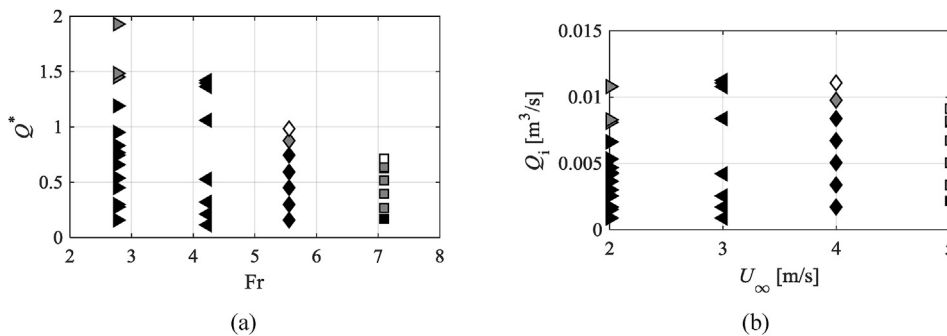


Fig. 4. Maps of the cavity topology boundaries as a function of Q^* vs. Fr (a), and Q_i vs. U_∞ (b) for $D_i = 20$ mm with $\delta \cong 52$ mm. The open symbols signify lambda, grey transitional and black filled a delta-topology. Figures adapted from Mäkiharju et al. (2017).

nominal sharp edges. The total mass-flow rate was measured for up to 500 Standard Liters Per Minute (slpm) with an Omega FMA5400 mass flow meter with manufacturer specified accuracy of $\pm 1.5\%$ of full scale ($\pm 3\%$ of full scale for fluxes below 100 slpm), and for over 500 slpm by

Omega FTB-939 flow meter with manufacturer specified accuracy of $\pm 1\%$ of reading. Additionally, flow to each of the injection pipes was independently measured by Venturi flow meters with the throat pressure drop measured with Omega PX138-001D5V pressure transducers. Given

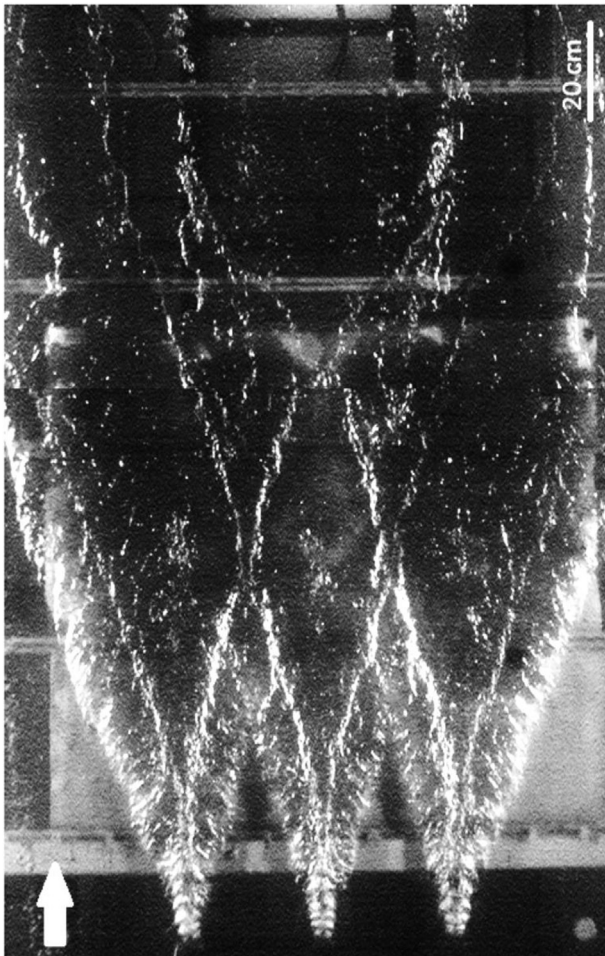


Fig. 5. Composite image of model's bottom viewed from below. This particular image is from preliminary experiments where gas was injected to $U_\infty = 2$ m/s cross-flow with 55 mm thick boundary layer from three 10 mm diameter holes spaced 25.4 cm apart. The liquid flow relative to the barge is from bottom to top, as indicated by the white arrow.

the propagation of uncertainty, especially for gas flux per hole, for the remainder of the paper gas flux uncertainty of $\pm 10\%$ of reading is assumed for the data. Fig. 2(a) shows the hole locations on the injector plate mounted immediately after the bow section as shown in Fig. 1. Fig. 2(b) lists the combinations of holes used. For the present work, the neighboring hole spacing, d , was 127 mm.

The primary measurements, in addition to gas flow rate and free-stream (*i.e.* tow tank carriage) speed were video recordings. Several GoPro Black Hero 3 cameras in watertight housings, and moving with the carriage, were utilized to record video at 1920×1080 resolution and 60 fps of the air pockets from above through the clear acrylic bottom of the model and from an oblique angle below water. In addition, a Vision Research Phantom V710 high-speed imager was installed inside a custom built watertight enclosure to the bottom of the tow tank to better visualize the flow as the model passed over. The quantitative observations reported, namely branch angles, are based on Phantom V710 recordings taken with 1280×800 resolution and 300 fps for duration of 787 frames, with $3328.5 \mu\text{s}$ exposure time. Lighting was provided at oblique angles by two custom built LED arrays, each with five 100W LEDs, installed underwater (opposite to each other) near the location on the Phantom V710 imager.

3. Single hole gas injection

As reported by Mäkiharju et al. (2017), when the gas is injected into a liquid cross-flow in boundary layer beneath the plate, at sufficient flux a

continuous gas jet emerges can penetrate the boundary layer. However, buoyancy forces the gas to travel toward the flow boundary, and initially a gas “pocket” is present immediately downstream (or around) the injector. This pocket develops downstream and two distinct flow topologies can be observed: “Delta”, where the gas spreads at a nominally constant angle until the layer thins out and breaks up, as shown in Fig. 3(a), and “Lambda”, where the gas also spreads at a nominally constant angle in two branches, but does not fill in the region between the branches, as shown in Fig. 3(b). A third type of topology could be denoted as transitional, as it resembles a mix between Delta and Lambda, with broken air layer (reminiscent of *transitional* air layer in terminology of Mäkiharju et al., 2012) filling the space between the branches as soon as they form immediately downstream of the initial gas pocket.

The spreading angle and topology (*i.e.* Delta vs. Lambda) of the gas pocket was found to depend on the free-stream speed, gas flux, gas injection angle, hole size and boundary layer profile, and these relative effects were studied both experimentally and numerically and discussed in Mäkiharju et al. (2017). Fig. 4 summarizes the observed topologies for a $D_i = 20$ mm hole (closest to the size used in present study). As for the present study, the Froude number is defined as

$$\text{Fr} = \frac{U_\infty}{\sqrt{g\delta}} \quad (3.1)$$

where U_∞ is the free-stream speed (in this case the tow tank's carriage speed), δ is the boundary layer thickness at the gas injection location in absence of gas injection (at y where $U = 0.99U_\infty$), and g is the gravitational acceleration. The non-dimensional gas flux is defined as

$$Q^* = \frac{Q_i}{U_\infty \delta^2} \quad (3.2)$$

where Q_i is the volumetric gas flux at the draft pressure. As will be later discussed in Section 4.1, it may also be useful to quantify injected gas flux as equivalent air layer thickness, t , defined as $t = Q_i / U_\infty S$, where S is the model span (a constant 1.5 m for present study). t would be the thickness for an uniform air layer in which gas is flowing with uniform velocity equivalent to the free stream velocity, U_∞ .

One could expect that gas injected from multiple holes to form an air layer for all cases where sufficient gas volume flux per span is injected for the given liquid flow speed. The required gas flux per unit span needed to achieve a stable air layer can also be estimated based on data summarized in Mäkiharju et al. (2012). At a minimum, this might also be expected to be the case for the delta topologies based on Fig. 4 when the holes are spaced apart a width that is less than the width of the gas pocket (formed from single injector) at the streamwise location where the air layer thins to the point of breaking. For a transitional or Lambda topology, based on map in Fig. 4, the formation of an air layer may be less certain, as the gas is not spread evenly but rather rolled up in the branches. Hence, the primary question for this multi-hole gas injection study is whether gas injected from multiple holes upon interacting will simply spread to an air layer as if injected from a continuous slot, roll up into larger structures upon merger of the branches, or otherwise fail to form an air layer, and how useful is single hole data to predict this outcome.

4. MULTI-HOLE gas injection results

When gas is injected from multiple holes, the general topology of the individual gas pockets emerging from the holes, and in the hole's immediate vicinity, remains qualitatively similar to that resulting from single-hole injection, as seen in Fig. 5 and compared to Fig. 3(a) (note that the conditions are not identical). However, closer inspection of Fig. 5 would also reveal that the interaction of the gas pockets alters the spreading angle of the gas branches even upstream of the point where they merge, when compared to topology of the gas pocket formed by similar injection parameters with single hole gas injection. Moreover, it is

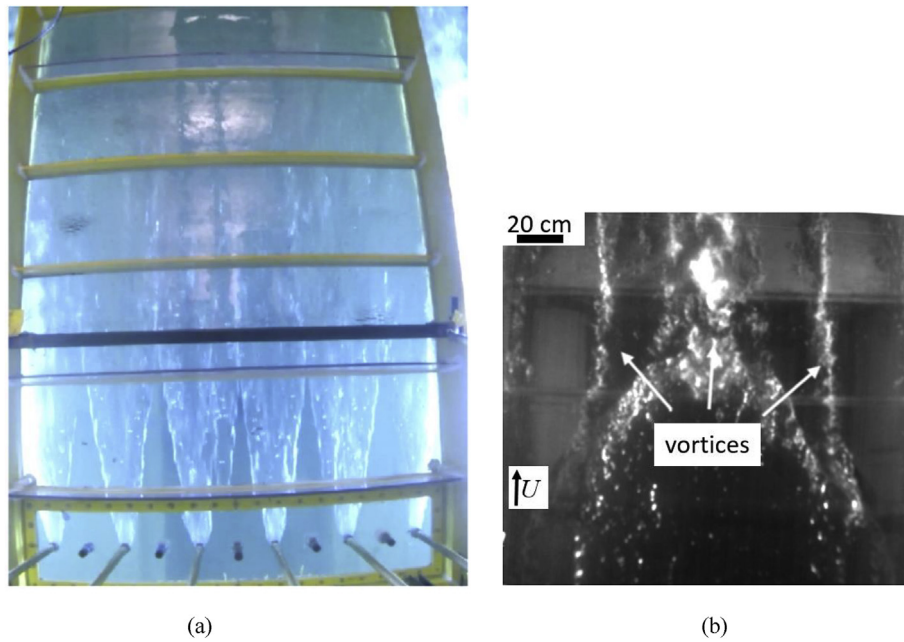


Fig. 6. Gas injected into a $U_\infty = 3$ m/s cross-flow at $Q_i = 43.7 \times 10^{-3}$ m³/s (i.e. $t = 9.7$ mm) from six holes separated by $2d$, showing (a) the flow from above and (b) from below (at location corresponding to a far downstream location in (a)) showing the gas rolled up into vortices as the air pocket closes.

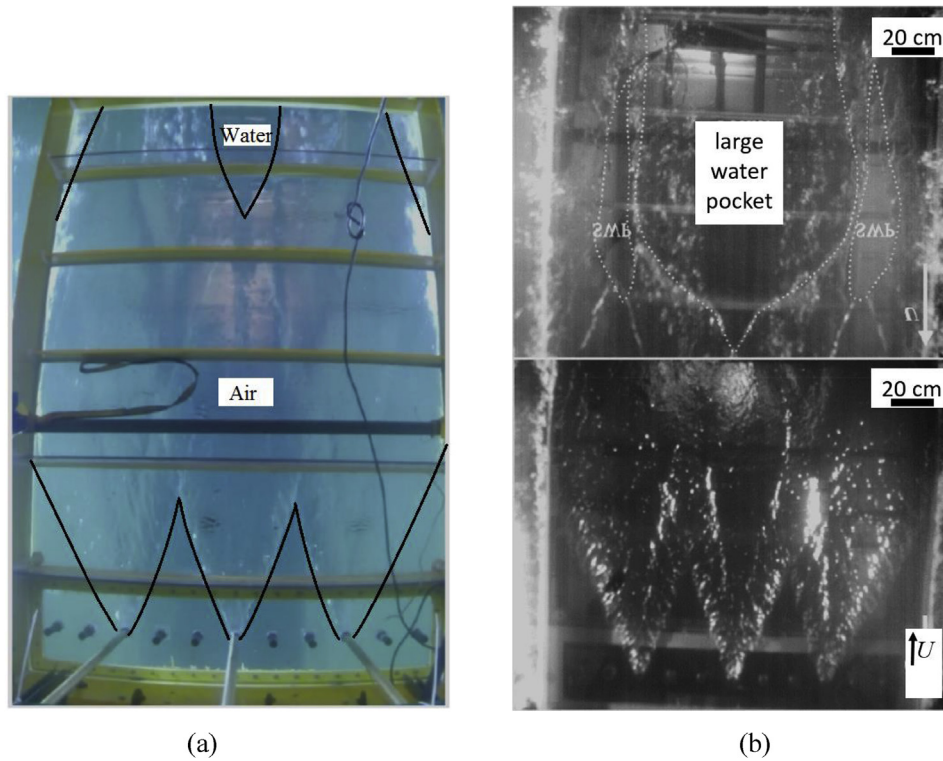


Fig. 7. Gas injected at $Q_i = 14.3 \times 10^{-3}$ m³/s to a $U_\infty = 2$ m/s flow (i.e. $t = 4.8$ mm) from three holes separated by $3d$. a) Top view through the acrylic bottom of the model and b) a stitched image showing view from below.

clear that the topology of the merged gas pockets can be quite complex (note the breakup at mid-span).

During the multi-hole gas injection experiments different gas fluxes and combinations of injection holes were explored, as shown in Fig. 2(b). The gas fluxes were balanced between all the holes based on measurements with the Venturi flow meters. Hence, the flux reported in latter discussion can be divided by number of holes utilized in that particular

case to have the value for the gas flux per hole. Fig. 5 shows a typical result for gas injection from 3 holes and the wedge topology expected based on the single hole data for this parameter combination can be seen near the point of injection. However, further downstream the individual cavities merge to form a non-uniform fractured gas layer, which may have ‘healed’ if the model were longer, may have formed a transitional air layer, or the gas may have been carried further away from the surface

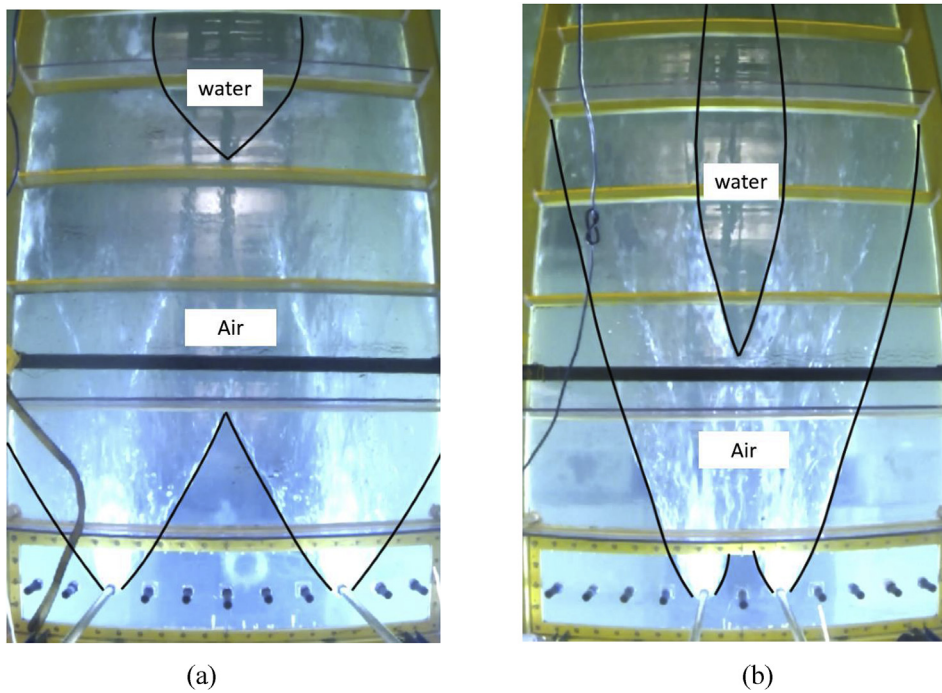


Fig. 8. Outlines of air cavities that were formed by the injected gas. Taken from top view videos for $U_\infty = 2$ m/s and $Q_i = 43.7 \times 10^{-3}$ m³/s (i.e. $t = 14.6$ mm). Conditions are nominally similar, except the two holes are (a) separated by $6d$, and (b) separated by $2d$.

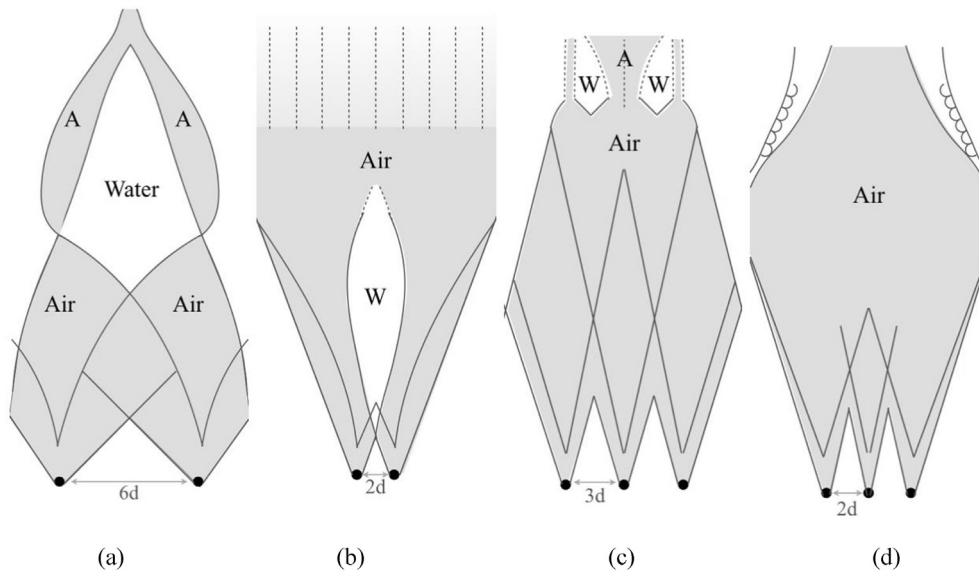


Fig. 9. Sketches of some of the typical air cavity shapes observed during the experiments. Flow resulting from gas injection of 42.2×10^{-3} m³/s into $U_\infty = 2$ m/s cross-flow (i.e. $t = 14.1$ mm) from two holes spaced $6d$ and $2d$ apart shown in (a) and (b), respectively. Flow resulting from gas injection of 21×10^{-3} m³/s into 3 m/s cross-flow (i.e. $t = 4.7$ mm) from two holes spaced $3d$ and $2d$ apart shown in (c) and (d), respectively.

and not contributed to reducing the frictional drag. We can also observe the perturbations propagating on the gas pocket surface at the angle of the branches on the free surface downstream of the location where the gas branches have merged.

Fig. 6(a) shows the initial growth of a gas cavity as air was injected into a $U_\infty = 3$ m/s cross-flow from six holes separated by 254 mm ($2d$) at $Q_i = 43.7 \times 10^{-3}$ m³/s (i.e. $t = 9.7$ mm) as seen through the clear bottom of the barge. This corresponds to approximately twice the gas flux expected to suffice for an air layer (Mäkiharju et al., 2012). However, Fig. 6(b) shows the termination of this gas cavity. But, instead of forming

an air layer the gas, starting from the edges of the gas layer, rolled up into vortices.

Similarly to Figs. 6 and 7 shows a topology resulting from gas injection from three holes separated by $3d$, with the outlines of the gas layer sketched out in (a). Once more, while at least a transitional air layer could be expected based on the topology resulting from injection of similar flux per span from a slot, the air layer breaks early, this time in the middle, and gas mostly appears to roll up into large streamwise structures located at $\sim 1/4$ and $\sim 3/4$ span. It should also be noted that for these cases (Figs. 6 and 7), minor leakage of gas over the strakes was suspected

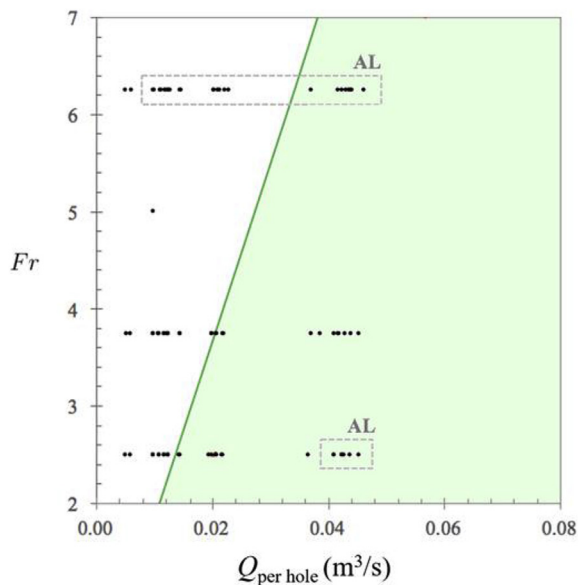


Fig. 10. Map of the topology as a function of Froude number and gas flux. An air layer (AL) was only formed by the end of the model in the cases enclosed in the dashed boxes. An air layer was considered formed, if a continuous layer of gas covered full span of the model at the end of the flat plate before strakes, shown in Fig. 1. The solid green line show the gas flux beyond which an air layer was expected to form on a smooth surface. (For interpretation of the references to colour in this figure legend, the reader is referred to the web version of this article.)

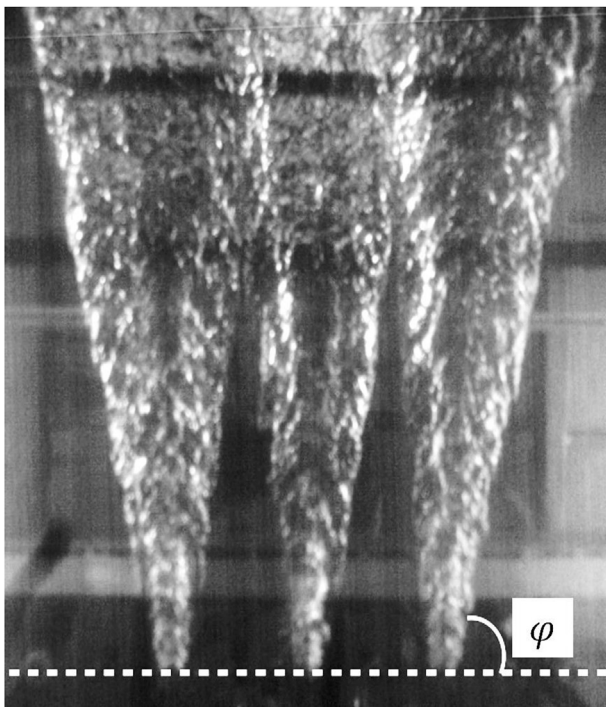


Fig. 11. The outer gas spreading angle (*i.e.* sweep angle) ϕ , is defined as shown in this figure.

based on video recordings taken from below and from the side at an oblique angle. However, often little to no leakage was observable, yet still no air layer was formed, even at fluxes much higher than should have been sufficient (*i.e.* $t > 7$ mm). Therefore, the failure to form an air layer was not simply explainable by leakage or gas around the strakes.

Fig. 8 shown another case where an air layer was expected to form, with all things being equal amongst (a) and (b) except for the spacing of the holes. The most striking difference is the significant difference in the spreading angle of the gas, albeit other differences can be discerned and are discussed below.

For the near injector region of the cavity, the outlines could be reliably defined from the view from above (as seen through the acrylic bottom), as shown in Figs. 7(a) and 8. However, combining observations from the cameras above and below the model enabled us to discern the overall air pocket shapes sketched in Fig. 9. It is interesting to note that while the case shown in Fig. 9(b) would seem to lead to an air layer (which may or may not have persisted had the model been longer) the same gas flux introduced from holes spaced further apart spaced holes, as sketched in Fig. 9(a), appears to show the is wrapped into vortices. And, over the length of the an air layer did not form. Note that while this model of finite span had strakes that based on review of video recorded from bottom and underwater from an oblique angle, appeared to prevent all (or most) of the air from escaping over the sides of the model for most cases studied, it is possible that non-negligible flux of air was driven out from the beam of the model and was simply not evident from the videos. Such air loss would alter the final developed of gas topology and could in many cases explain why an air layer failed to form at the relatively high fluxes (*i.e.* even when $t > 7$ mm).

As discussed in context of partial cavities by Matveev (2007), the gas-liquid interface over the finite span of the model can become highly three dimensional with complicated the flow topology. In case of cavities formed downstream of a deep step, Matveev (2007) and Mäkiharju et al. (2013) found that complex wave patterns formed on the cavity surface. Not surprisingly, in similar manner as evident in present work (*e.g.* Fig. 9), finite span of the model for air layer formed from discrete injection points complicates the analysis. Besides the finite span between the strakes, complications may arise from the non-uniformity of the flow beyond the model span.

In some cases, a water patch appeared in the middle of the model (*e.g.* in Fig. 9(a) and (b)). This topology is similar to that observed for single point injection when the columns of gas emerging from the orifice pushed the liquid flow over the middle away from the surface. Downstream of the orifice, the liquid flow follows the gas returning to the surface under effect of gravity, and this liquid flow with momentum towards the surface promotes cleaving of the air cavity. Consequently, stable gas branches may form in single orifice injection case, where this sometimes even leads to the absence of gas between the branches (*i.e.* the so-called Lambda topology) as seen in Fig. 3(b).

The gas jet penetration depth at the site of injection may explain some of the different topologies depicted in Figs. 5–9, and the dependence on number of holes utilized to introduce the same total gas flux. As evident in Fig. 9(a) vs. (b), the two-injector configuration with $6d$ spacing shows a smaller sweep angle (wider spreading angle that is a benefit for the air-layer drag reduction), with a large water pocket that forms before the end of the flat plate (a negative outcome for air-layer drag reduction). When a third injector is added with spacing $3d$, even with reduced gas flux, the spreading angle is larger but now the large water pocket in the middle does not appear (see Fig. 9(c)). Lack of a water pocket may be due to a smaller jet penetration depth. As injectors are added and overall gas flux per span kept constant, the flux per hole is reduced. Based on previously published single hole results, this would decrease the gas penetration depth.

Also, related to jet penetration depth is the formation and strength of a liquid junction vortex that forms at the location of gas injection. This junction type vortex (*i.e.* horseshoe vortex) forms and persists far downstream in front of the gas branches, and may also play a role in determining the gas spreading angle. And, as with the single hole gas injection, this can be expected to be the case also multi-hole injection. Additionally, as cavities originating from different injectors interact, this is expected to potentially modify the pressure in the cavity (or branches), which in turn can also alter the branch angle see analysis of force balance

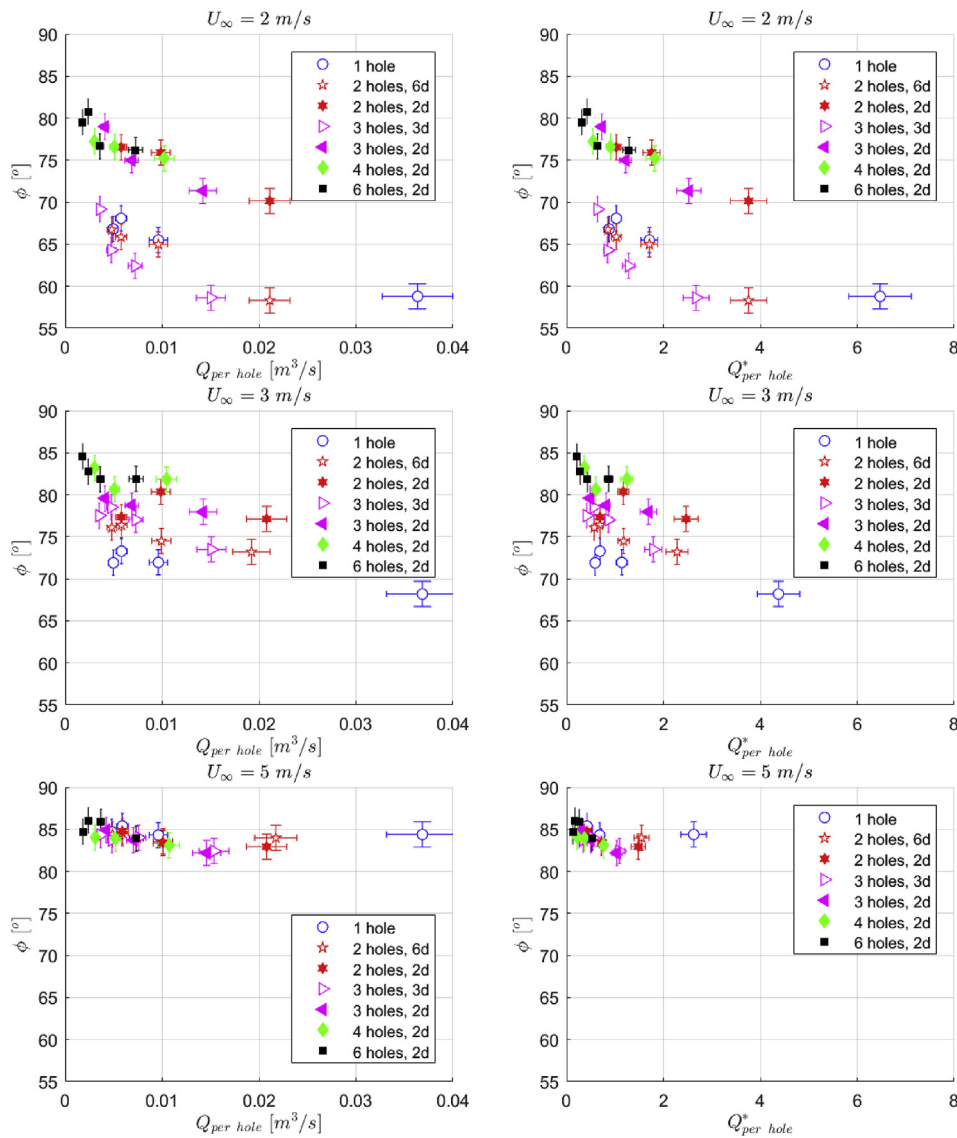


Fig. 12. Outer gas spreading angle, as defined in Fig. 11. From top to bottom, for liquid cross-flow of $U_\infty = 2, 3$ and 5 m/s, respectively. Figures on the right show clearly that even in these were superimposed, the data would not simply collapse with Q^* alone.

on branch of Mäkiharju et al. (2017).

4.1. When to expect an air layer

As previously discussed, gas injected beneath a horizontal surface and into a liquid cross-flow from a single hole was found to spread at a nominally constant angle that is primarily dependent on the liquid free-stream speed and gas jet volume flow rate (Mäkiharju et al., 2017). With sufficient gas per span injected from multiple holes, the gas could spread at somewhat similar angles to form an air layer. In order to determine the minimally sufficient flux, we refer to data from ALDR experiments that utilized a continuous slot to introduce the gas (summarized in Mäkiharju et al., 2012). The nominal air layer thickness can be defined as $t = Q_i / U_\infty S$, where Q_i is the gas flux at the draft's pressure, U_∞ is the free-stream speed of liquid and S is the model span. Based on experimental data at 6.8 m/s smooth and rough surfaces necessitate a nominal air layer thickness, t_{\min} , to be equal or greater than 4 and 7 mm, respectively. As the experimental data was not available at lower speeds, t_{\min} was assumed to remain constant for $0 \leq U_\infty \leq 6.8$ m/s, and the t_{\min} value for smooth surfaces is shown by the green line in Fig. 10. Fig. 10 presents gas flux in units of flux per hole, instead of average flux per span or related

unit such as t , as flux per hole, hole size, and hole angle will potentially affect whether an air layer results from multihole injection. (A related discussion on topology resulting from single hole gas injection to liquid crossflow was provided in Mäkiharju et al., 2017.)

A somewhat surprising finding seen in Fig. 10 is that for the present model an air layer was sometimes not achieved even though the critical gas flux based on slot injection was exceeded by factor of two or more, while in other cases at high Froude numbers it appears an air layer was achieved at gas fluxes much less than expected critical flux. For the case where more gas was needed, this result could be due to the flow perturbations caused by discrete gas injection resulting in the gas rolling up as the branches interacted. Also, while this model of finite span had strakes that appeared to keep most of the air from escaping, it cannot be said with certainty that air loss from the sides or potentially non-uniform spanwise flow over the model did not alter the outcome of the experiments. Nor can we preclude the possibility that on a longer model the air layer would have “healed” further downstream.

For the case where less gas was needed than expected, given the model's rather short flat bottom (3.4 m long model mid-section), the air layer initially formed may not have persisted if the model been longer. However, the assumption that t_{\min} is constant for $0 \leq U_\infty \leq 6.8$ m/s

(below speeds where data was available), may also be questioned.

4.2. Gas spreading angle

It is also instructive to compare the gas spreading angle in the multi-hole case versus that observed for single holes, and for multi-hole with varying hole spacing, as this may be an indication of the air cavity pressure as discussed in Mäkiharju et al. (2017). Fig. 11 shows how spreading angle was defined, and Fig. 12 shows the measured outer angles for $U_\infty = 2, 3$ and 5 m/s multi-hole experiments. The angle was measured from multiple frames of video. The uncertainty was estimated as $\pm 1.5^\circ$ and principally attributed to the fluctuations of the edge of the gas branch that is presumably still related to the puffing previously discussed in Mäkiharju et al. (2017). The normalized gas flux, Q^* , is based on Eq. (3.2)

Note that as the proximity of the holes is decreased as the sweep angle increased, indicating that there may have been a lower cavity over pressure due to change in cavity closure condition. The variation of angle with spacing of holes could also be related to changes in the junction vortex near the location of injection, which affected the sweep angle in the single hole case. An increase in gas flux or decrease in free-stream speed led to a decrease in sweep angle (wider air layer), as was also the case for single hole injection. Interestingly, however, it appears an increase in hole spacing for otherwise fixed flow and injection conditions had a similar effect. Further study (ideally a joint experimental and numerical effort) would be needed to make clearer conclusions on the relative roles of the different mechanisms.

5. Summary

Topology of gas pockets resulting from gas injection from multiple holes into a liquid cross-flow was examined, and the results were compared to gas injection from a single orifice. Complex gas-pocket topologies were observed for the single point injection as discussed in Mäkiharju et al. (2017). And, it was observed in the present study gas injected through multiple holes placed in the beamwise direction to the incoming flow also exhibited similar features, such as the formation of gas branches in a V-shaped pattern. However, the presence of multiple holes additionally led to the complex interaction of the injected gas pockets. These interactions, along with three-dimensional features of the external flow (particularly that due to vortices near the model corners) is thought to help explain some of the complex flow patterns observed.

A motivation for the study was to determine if discreet injection of gas through multiple holes can lead to the production of an air layers. The present results indicate that, under certain conditions (e.g. often corresponding to the Lambda geometry of the single hole case) the gas injected from multiple holes *does not* spread into an air layer over the length of the model. Rather, the gas rolls up into vortices formed as part of the injection process or due to the presence of finite beam of the model, as shown e.g. in Fig. 6(b). However, stable air layers were observed in some cases (e.g. Fig. 9(b)), and in a subset of cases the gas flux needed to form

the layer was *less* than that expected based on injection from a continuous spanwise slot (see Fig. 10). In order to confirm these somewhat surprising, and in some cases fortuitous results, additional experiments should be conducted. To enable stronger conclusions, the experimental conditions would ideally cover a wider range of flow parameter, utilize a model with a wider beam and longer overall length, and incorporate additional quantitative measurements (e.g. to measure the cavity pressure at multiple points and quantify external liquid flow strictures).

Acknowledgements

The authors gratefully acknowledge the thorough work done by visiting undergraduate students Ms. Helene Ungerman and Mr. Pierre Lamache, who aided in the conduct of the experiments, preliminary analysis of the data, and the creation of several figures employed in this work. The assistance provided by Dr. Inho Lee is gratefully acknowledged. This work was funded in part by the Office of Naval Research under grant N00014-14-1-0292, Dr. Ki-Han Kim program manager.

References

- Ceccio, S.L., 2010. Friction drag reduction of external flows with bubble and gas injection. *Annu. Rev. Fluid Mech.* 42, 183–203.
- Elbing, B.R., Mäkiharju, S., Wiggins, A., Perlin, M., Dowling, D.R., Ceccio, S.L., 2013. On the scaling of air layer drag reduction. *J. Fluid Mech.* 717, 484.
- Gokcay, S., Insel, M., Odabasi, A.Y., 2004. Revisiting artificial air cavity concept for high speed craft. *Ocean. Eng.* 31 (3), 253–267.
- Insel, M., Gokcay, S., Helvacioğlu, I.H., 2010. Flow analysis of an air injection through discrete air lubrication. In: *International Conference on Ship Drag Reduction*, Paper No. 13.
- Kumagai, I., Takahashi, Y., Murai, Y., 2015. Power-saving device for air bubble generation using a hydrofoil to reduce ship drag: theory, experiments, and application to ships. *Ocean. Eng.* 95, 183–194.
- Lay, K.A., Yakushiji, R., Mäkiharju, S., Perlin, M., Ceccio, S.L., 2010. Partial cavity drag reduction at high Reynolds numbers. *J. Ship Res.* 54 (2), 109–119.
- Lee, I.R., 2015. Scaling of Gas Diffusion into Limited Partial Cavity and Interaction of Vertical Jet with Cross-flow beneath Horizontal Surface. Ph.D. dissertation. University of Michigan.
- Mahesh, K., 2013. The interaction of jets with crossflow. *Annu. Rev. Fluid Mech.* 45, 379–407.
- Matveev, K.I., 2007. Three-dimensional wave patterns in long air cavities on a horizontal plane. *Ocean. Eng.* 34 (13), 1882–1891.
- Mäkiharju, S.A., Perlin, M., Ceccio, S.L., 2012. On the energy economics of air lubrication drag reduction. *Int. J. Nav. Archit. Ocean Eng.* 4 (4), 412–422.
- Mäkiharju, S.A., Elbing, B.R., Wiggins, A., Schinasi, S., Vanden-Broeck, J.M., Perlin, M., Ceccio, S.L., 2013. On the scaling of air entrainment from a ventilated partial cavity. *J. Fluid Mech.* 732, 47.
- Mäkiharju, S.A., Lee, I.H.R., Filip, G.P., Maki, K.J., Ceccio, S.L., 2017. The topology of gas jets injected beneath a surface and subject to liquid cross-flow. *J. Fluid Mech.* 818, 141–183.
- Murai, Y., 2014. Frictional drag reduction by bubble injection. *Exp. fluids* 55 (7), 1773.
- Park, H.J., Oishi, Y., Tasaka, Y., Murai, Y., 2016. Void waves propagating in the bubbly two-phase turbulent boundary layer beneath a flat-bottom model ship during drag reduction. *Exp. Fluids* 57 (12), 178.
- Perlin, M., Ceccio, S., 2014. *Mitigation of Hydrodynamic Resistance: Methods to Reduce Hydrodynamic Drag*. World Scientific.
- Vigneau, O., Pignoux, S., Carreau, J.-L., Roger, F., 2001a. Influence of the wall boundary layer thickness on a gas jet injected into a liquid crossflow. *Exp. Fluids* 30, 458–466.
- Vigneau, O., Pignoux, S., Carreau, J.-L., Roger, F., 2001b. Interaction of multiple gas jets horizontally injected into a vertical stream. *Turbul. Combust.* 66, 183–208.